

**Integrated Seismological and Tectonic Studies of the
Loma Prieta Earthquake Sequence**

Agreement No. 14-08-0001-G1831

A. Lerner-Lam, W. Menke, D. Simpson, W.Y. Kim, L. Seeber, S. Hough, and K. Fischer
Lamont-Doherty Geological Observatory
Palisades, N.Y. 10964

(914) 359-2900

Overview

Following the October 17, 1989 Loma Prieta earthquake, an array of 22 IRIS/PASSCAL (Incorporated Research Institutions for Seismology/Program for Array Studies of the Continental Lithosphere) instruments was deployed in the epicentral area in the Santa Cruz Mountains (Figure 1; Simpson et al., 1989). Eleven of these instruments were installed by October 22; the remainder were installed before October 29 of 1989. The instruments remained in place through November.

We have undertaken an integrated approach for using aftershock recordings to examine the structure of the Southern Santa Cruz Mountains segment of the San Andreas Fault (SAF). Both IRIS/PASSCAL and CALNET phase data have been used to relocate events and to obtain focal mechanisms for over 1000 Loma Prieta aftershocks. The IRIS/PASSCAL waveform recordings have been used to study both the stress drop of a subset of aftershocks and the regional attenuation structure. Studies of both seismicity and aftershock waveforms are used to elucidate the complex fault zone structure in the vicinity of the Loma Prieta rupture and to understand the mainshock-aftershock rupture processes.

Data Processing

Aftershock waveform data were recorded on 3-component L-22 2-Hz velocity sensors paired with IRIS/PASSCAL RefTek recorders. Sampling was at 200 sps, with high- and low-gain recordings. Triggering was via STA/LTA comparisons with a threshold of 4.5. Instrument response is theoretically flat to velocity between ≈ 3 and 100 Hz; Menke et al. (1991) bench-tested the sensors following the aftershock deployment and showed the L-22 to be free of spurious resonances only for frequencies below 25 Hz.

The IRIS/PASSCAL data set consists of 763 $m \geq 1.5$ events that have been associated with events in the CALNET catalog. Preliminary CALNET event hypocenters were relocated using path-dependent station corrections generated using 20 years of CALNET phase data (Seeber and Armbruster, 1990). Visual inspection of waveforms suggest that these relocations can provide a significant improvement in (at least) relative event locations. The correlation between hypocenter proximity and waveform similarity improved significantly from the preliminary to the relocated hypocenters.

Results I: Structure of the Fault Zone from Focal Mechanism Observations

First-motion focal mechanisms were determined for more than 200 aftershocks in a volume beneath the PASSCAL array deployment extending from the surface to 20 km depth. First motions were obtained from both the PASSCAL and CALNET arrays but the densely-spaced PASSCAL array provided improved coverage of the focal sphere for the shallowest aftershocks. Focal mechanisms were determined using a grid-search algorithm and were assessed using a statistical model based on the binomial distribution (Guo et al., 1990).

The directions of the compressional (P) axes of 151 well-determined focal mechanisms were averaged in 2 km-thick depth intervals and the variability was determined by computing the standard deviation of the P-axis azimuth. About 70% of the P-axes of events below 4 km lie within a 90-degree quadrant with a mean consistent with the main shock focal mechanism. The shallower aftershocks are also consistent with the P-axes azimuth of the main shock, but the scatter in azimuth is reduced by about 50%. Moreover, the hypocenters of the shallow aftershocks do not appear to lie on the extension of a plane defined by the deeper aftershocks and are scattered in a broader zone.

The lateral distribution of both aftershock and pre-Loma Prieta focal mechanisms provide further insight into the nature of fault complexity (e.g. Seeber and Armbruster, 1990). When viewed down-dip (Figure 1b), pre-Loma Prieta hypocenters of the Lake Elsmar source and 1989 aftershocks are spatially distinct. In fact, they seem to be mutually exclusive, suggesting that structures that were active during the precursory period were inactive during the aftershock sequence (with the prominent exception of the northern creeping section of the SAF).

Pre-Loma Prieta hypocenters are clustered within the foot wall of the Loma Prieta rupture, on a set of secondary faults that branch off the main fault (Figure 1). Like the main fault, these secondary faults move right-laterally with a large component of reverse motion, but, unlike the main rupture, they dip northeast and the motion is consistently up on the northeast side. The seismicity provides a precursory signal with a strong burst close in space and time to the nucleation point of the main shock (i.e. the Lake Elsmar events). This seismicity originates from secondary faults antithetic to the main rupture. Perhaps the most significant aspect of the seismicity during 20 years prior to Loma Prieta is the absence of earthquakes on the upcoming rupture (Figure 1b).

While not detracting from the hypothesis of total stress drop, an investigation into the 3-dimensional variability of aftershock focal mechanisms does yield systematic patterns that suggest interactions with neighboring elements of the fault zone. Focal mechanisms tend to be similar to each other and to the main shock mechanism--a mixture of reverse and right-lateral slip--along the southeastern side and, to a lesser extent, along the upper northwestern rim of the rupture. These are the portions of the rupture rim that intersect the main shock slip vector at large angles.

The persistent intense aftershock zone along the lower southeast rim suggest post-seismic creep down-dip of that zone. Many of the mechanisms share with the main shock similar slip vector projections on the rupture plane, but have distinct nodal planes. These events probably rupture secondary faults within the fault zone which accommodate an overall kinematics similar to the main shock.

Strike-slip dominates on the southeast side, at the juncture with the creeping segment, reverse slip dominates on the northwest side, toward the juncture with a locked segment. This pattern of slip resembles the slip distribution in the main shock rupture resolved from near-field seismograms. This asymmetric distribution of slip is consistent with the 1989 rupture being confined on the northwest by a locked and highly stressed portion of the fault and on the southeast by a weak and creeping portion of the fault.

Results II: Structure of the Fault zone from Waveform Analysis

Previous studies have shown that it is difficult to independently resolve source properties of small earthquakes and attenuation. We have analyzed a subset of the IRIS/PASSCAL data set using an empirical Green's function method, where-by the recording of a small event is used to deconvolve path and site effects from the recording of a nearby larger event (Hough et al., 1991). In a pilot project using data from a preliminary data set containing 55 events, we find 4 pairs of events suitable for empirical Green's function analysis. We also analyze waveforms from an additional 8 events that occur close to these pairs.

We show that the largest aftershocks are well-modelled by an omega-square source spectrum and we obtain estimates of the *P*-wave corner frequency for a total of 15 events. Brune

stress drops are observed to have no systematic variation over the range of moments spanned by the data set, down to 10^{19} dyne*cm. There is a suggestion that aftershocks that occurred outside the mainshock rupture have higher stress drops than those that occurred within the main shock rupture.

A $m_l=3.4$ foreshock in the subsequence associated with the 4/18/90 $m_l=5.4$ Watsonville earthquake yields a stress drop estimate of 820 bars. This value is well outside the stress drops obtained for all other events (6 to 266 bars).

Site-specific attenuation parameters suggest large lateral and vertical heterogeneity in P -wave attenuation structure (Figure 2). Station HOLY, in a valley near the surface trace of the SAF, is characterized by low Q values, while stations to the north of the aftershock zone are characterized by the highest Q values. Paths that travel to the surface along strike of the main shock rupture plane to station HOLY yield Q values of 75-90, while paths that travel through the hanging wall yield Q values closer to 150. These low- Q values can not be plausibly explained by attenuation within very shallow near-surface sediments. Low whole-path Q values are obtained from both shallow and deep events whose paths traverse along strike of the fault zone, suggesting that attenuation above 4-6 km is comparable to that in the fault zone at depth. This further suggests that a significant fault zone continues from the top of the main shock rupture to the surface.

Whole-path Q values for paths 50-70 km long are significantly higher than estimates for paths 20-40 km long (e.g. 275-850 vs 70-290, respectively), suggesting a significant increase of Q with depth.

We also conducted a study of spectral ratios from pairs of stations in the PASSCAL array using one station near the fault trace and one west of it (Menke, 1990). Anomalously low spectral ratios, indicating anomalously high attenuation, are observed for a substantial number of events, especially events in the deeper half of the main shock rupture. These results also suggest high attenuation along the fault zone.

Velocity Structure from Loma Prieta Recordings

We have conducted synthetic experiments using the actual distribution of sources and receivers at Loma Prieta (Caress et al., 1990). These studies show that the dense sampling of the aftershock zone is sufficient to resolve heterogeneities on the scale of a 1-km thick low-velocity zone. We trace rays through a 3-dimensional model that contains low velocities in the volume defined by the aftershock seismicity. Raypaths, travel times, and their partial derivatives are calculated analytically. We orthogonalize the inverse problem with respect to the source location and solve for the velocity perturbation that minimizes the sum of the 2-norm of the travel-time misfit. We invert the resulting travel times (assigned Gaussian-distributed errors with a standard deviation of 0.05 s) and retrieve a well-resolved image of the original structure.

Summary and Conclusions

We suggest that the high scatter in P -axis orientations within the main shock rupture and the difference between on-rupture and off-rupture stress drop are consistent with a model in which the Loma Prieta event removed most of the stress load within the mainshock rupture as delineated by the early aftershocks. From the reduced variability in the orientation of shallow P -axes, the high stress drop of off-rupture events, and the inferred 3-dimensional attenuation structure, we conclude that increased or significant residual stress may exist on a complex system of shallow faults. Our results may be diagnostic of a situation in which the Santa Cruz segment of the San Andreas is segmented down-dip and can produce several distinct characteristic earthquakes. Further, the shallow stress may be relieved by post-main shock seismic or aseismic movement on a complex system of shallow thrust and strike slip faults.

Publications

- Caress, D.W., K.M. Fischer, and A. Lerner-Lam (1990). Tomographic imaging of the Loma Prieta rupture zone, (abstract), *Trans. Am. Geophys. U.* 71, 562.
- Guo, H., A. Lerner-Lam, J.G. Armbruster, and Z. Tu (1990). Variability of small-aftershock focal mechanisms in the Loma Prieta rupture zone from PASSCAL and CALNET data, (abstract), *Trans. Am. Geophys. U.*
- Hough, S.E., L. Seeber, A. Lerner-Lam, J. Armbruster, and H. Guo (1991). Empirical Green's function analysis of Loma Prieta aftershocks, submitted to *Bull. Seism. Soc. Am.*
- Menke, W. (1990). Evidence for high attenuation along the San Andreas fault in the Loma Prieta aftershock zone (abstract), *Trans. Am. Geophys. U.* 71, 1471.
- Menke, W., L. Shengold, H. Guo, G. Hu, and A. Lerner-Lam (1991). Performance of the short-period geophones of the IRIS/PASSCAL array, *Bull. Seism. Soc. Am.* 81, 232-242.
- Seeber, L. and J.G. Armbruster (1990). Fault Kinematics in the 1989 Loma Prieta rupture area during 20 years before that event, *Geophys. Res. Lett.* 17, 1425-1428.

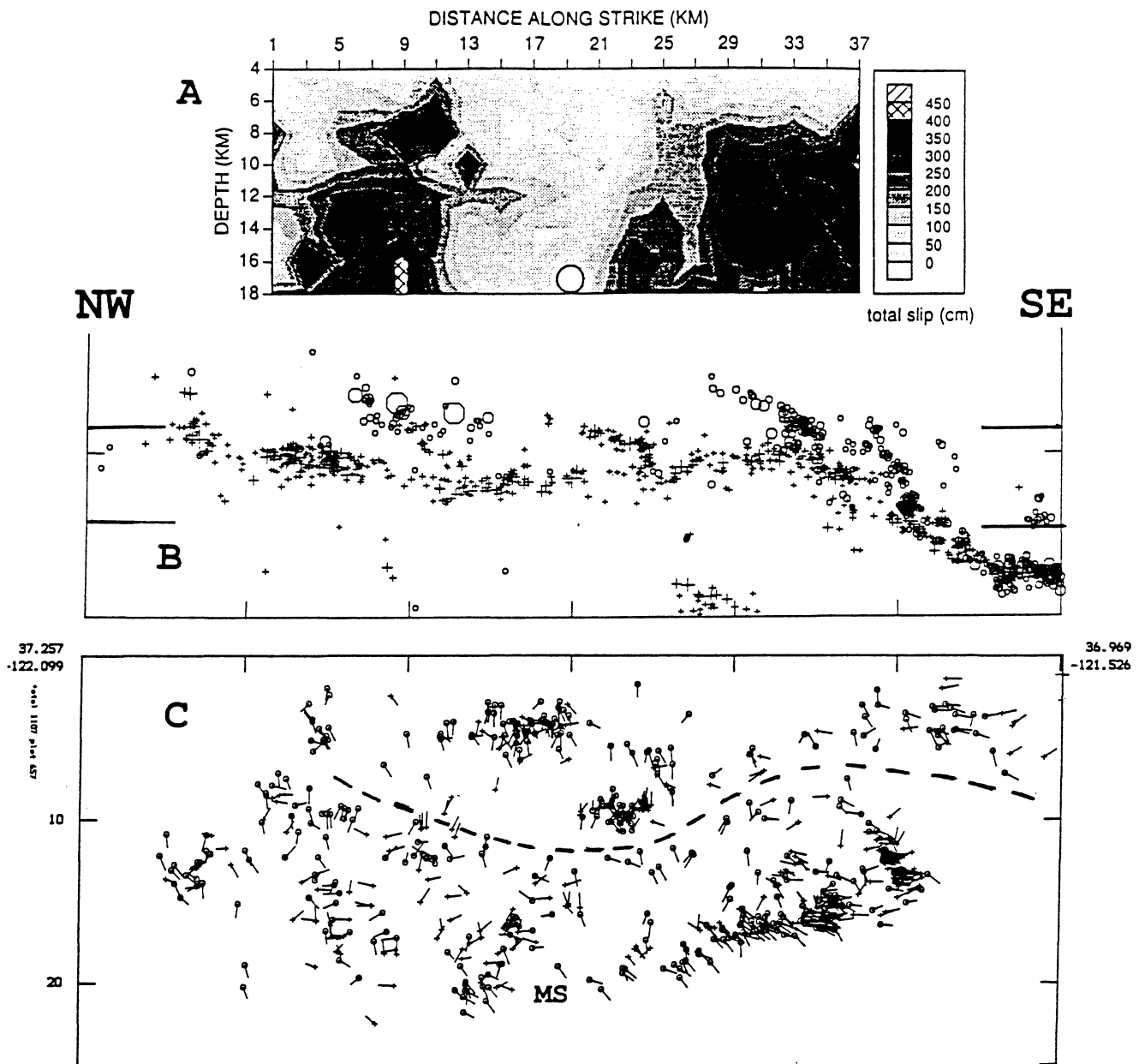


Figure 1. Face (C) and dip (B) view of rupture. Dip view shows hypocenters (+’s are aftershocks; o’s are before the main shock). Face view shows slip vectors. The narrow band selected for the face view (6 km wide; indicated in dip view) includes some seismicity clearly off the main fault; most seismicity above dashed line is not on the main fault. Dip view includes only seismicity deeper than about 6 km. The two $M \approx 5$ Lake Ellsman events are part of the western-most cluster north of the rupture. Compare with total slip distribution for the main shock (A; from Steidl et al., 1991; sections are properly aligned and at the same scale). Segmentation of rupture surface suggested by seismicity (e.g. dip view) shows correlation with zones of distinct slip.

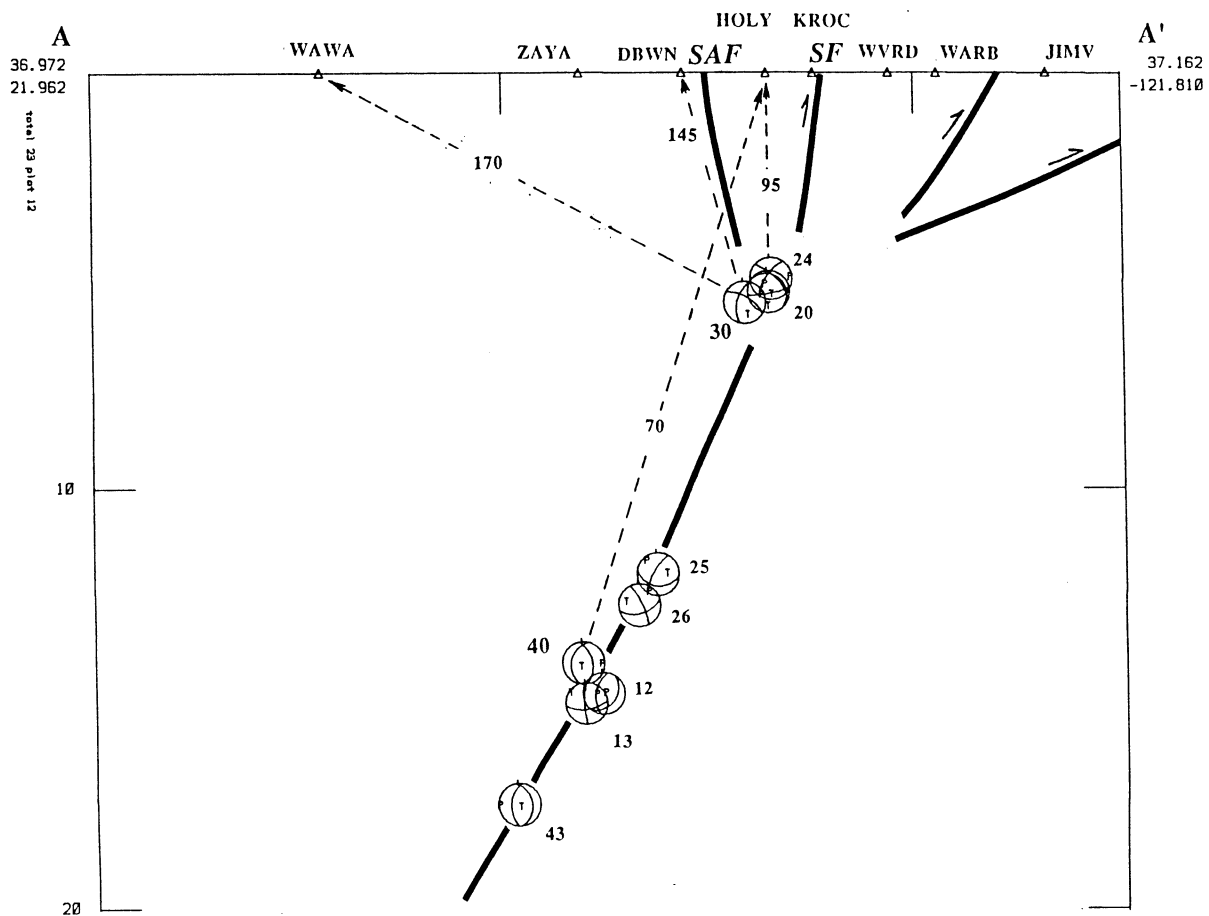


Figure 2. Cross section across Loma Prieta rupture including faults (from Seeber and Armbruster, 1990), hypocenters and focal mechanisms of the events analyzed, and stations (triangles). Whole-path P -wave Q values are shown for several of the source-receiver paths analyzed. Projected raypaths sketched approximately for illustration. For comparison, raypaths from the southern-most events to the northern most stations yield Q values of 550-850.